CDF note 9246

Search for new particles decaying to dijets in $p\bar{p}$ collisions at $\sqrt{s} = 1.96$ TeV

The CDF Collaboration
URL http://www-cdf.fnal.gov
(Dated: March 24, 2008)

We present a search for dijet mass resonances using 1.13 fb^{-1} of the CDF Run II data. No evidence for new particle decaying into dijets is found, and 95% C.L. limits are put on new particle production.

I. INTRODUCTION

One of potential new physics signatures is a narrow resonance in the dijet mass spectrum. Many classes of beyond-the-standard-model scenarios predict the presence of new massive particles that decay into two energetic partons (quarks and gluons), and they are expected to produce a resonant structure in the dijet mass spectrum. Such particles include excited quarks ($q^* \to qg$) [1], axigluons ($A \to q\bar{q}$) [2], color octet techni-ρ ($\rho_T \to q\bar{q}, gg$) [3], W' ($W' \to q\bar{q}'$), Z' ($Z' \to q\bar{q}$), diquarks in the string-inspired E_6 model [$D(D^c) \to (qq)\bar{q}\bar{q}$] [4], and Randall-Sundrum gravitons ($G \to q\bar{q}, gg$) [5]. Searches for resonances in the dijet mass spectrum is challenging due to large contribution from direct two-jet production via quantum chromodynamics (QCD); however, the previous observation of W and Z bosons decaying into dijets by the UA2 Collaboration showed a feasibility of finding dijet mass resonance at the hadron colliders [6]. In the past, the UA2 [7], CDF [8, 9] and DØ [10] experiments searched for resonances in the measured dijet mass spectrum and set limits on their production. In this note, we present a search for new massive particles decaying into dijets in $p\bar{p}$ collisions at $\sqrt{s} = 1.96$ TeV using 1.13 fb^{-1} of data collected with the CDF II detector at the Fermilab Tevatron.

II. THE CDF DETECTOR

The CDF II detector is described in detail elsewhere [11]. Here, those components that are crucial to this search are briefly described. The central detector consists of a silicon vertex detector (SVX II), composed of double-sided microstrip silicon sensors arranged in five cylindrical shells of radii between 2.5 and 10.6 cm, inside a cylindrical open-cell drift chamber of 96 layers organized in 8 superlayers with alternating structures of axial and $\pm 2°$ stereo readout within a radial range between 40 and 137 cm. Surrounding the tracking detectors is a superconducting solenoid magnet which provides a 1.4 T magnetic field. The sampling calorimeters surround the tracking system with a projective tower geometry and measure the energy of interacting particles.

In the central region ($|\eta| < 1.1$), the calorimeter consists of 48 modules, segmented into towers of granularity $\Delta\eta \times \Delta\phi \approx 0.1 \times 0.26$. The central electromagnetic calorimeter (CEM) is a lead-scintillator calorimeter with a depth of about 18 radiation lengths; the central hadron calorimeter (CHA) is an iron-scintillator calorimeter with a depth of approximately 4.7 interaction lengths. The energy resolution of the CEM for electrons is $\sigma(E_T)/E_T = 13.5\%/\sqrt{E_T(\mathrm{GeV})} \oplus 2\%$ while the average energy resolution of the CHA for charged pions is $\sigma(E_T)/E_T = 50\%/\sqrt{E_T(\mathrm{GeV})} \oplus 3\%$. The forward region, $1.1 < |\eta| < 3.6$, is covered by the "Plug Calorimeters" consisting of lead-scintillator for the electromagnetic section and iron-scintillator for the hadronic section. The region between the central and forward calorimeters, $0.7 < |\eta| < 1.3$, is covered by an iron-scintillator hadron calorimeter with similar segmentation to the central calorimeter.

III. DATASETS, JET CLUSTERING, EVENT SELECTION AND JET CORRECTIONS

This search uses a data sample corresponding to an integrated luminosity of 1.13 fb^{-1} collected between February 2002 and February 2006. The jet data used in this search were collected using four trigger paths. The Level 1 trigger requires a calorimeter trigger tower, consisting of pre-defined pairs of calorimeter towers adjacent in η, to have $E_T > 5$, 10, or 20 GeV depending on the specific trigger path and data-taking period. At Level 2, the calorimeter towers are clustered using a nearest neighbor algorithm. Four trigger paths with cluster $E_T > 15$, 40, 60, and 90 GeV are used. Events in these paths are required to pass jet $E_T > 20$, 50, 70, and 100 GeV thresholds at Level 3, where the clustering is performed using a cone algorithm with a cone radius $R_{cone} = 0.7$. These four trigger paths are referred to as jet20, 50, 70, and 100, respectively. The jet20, 50 and 70 triggers are prescaled to avoid saturating the bandwidth of the trigger and data acquisition system. After prescaling, the jet20, 50, 70, and 100 triggered data samples correspond to 1.44, 32.5, 143 pb^{-1} and 1.13 fb^{-1}, respectively. These trigger samples are used to form the dijet mass spectrum above 180, 241, 321 and 427 GeV/c^2, respectively, where the trigger efficiencies are higher than 99.8%.

Offline, jets are reconstructed from the energy depositions in the calorimeter towers with $p_T > 0.1$ GeV/c^2. Jets are clustered by the cone-based Midpoint jet clustering algorithm with cone radius $R_{cone} = 0.7$ [12, 13] with the splitting/merging fraction of 0.75. Cosmic ray events and beam-related background events are removed by applying a cut on missing-E_T significance, $\not{E}_T/\sqrt{\sum E_T}$ [14]. The cut threshold varies with the highest-p_T jet in the event and is defined by $\not{E}_T/\sqrt{\sum E_T} < \min(3 + 0.0125 \times p_T^{max}, 6)$ where p_T^{max} is the maximum raw jet p_T in the event in unit of GeV/c. The missing-E_T significance cut is about 100% efficient for low dijet mass (m_{jj}) and the efficiency decreases to about 95% at $m_{jj} = 1200$ GeV/c^2. In order to ensure that the jet energy is well measured, the event vertex is required to be within 60 cm of the center of the detector along the beam direction. The efficiency for this cut is

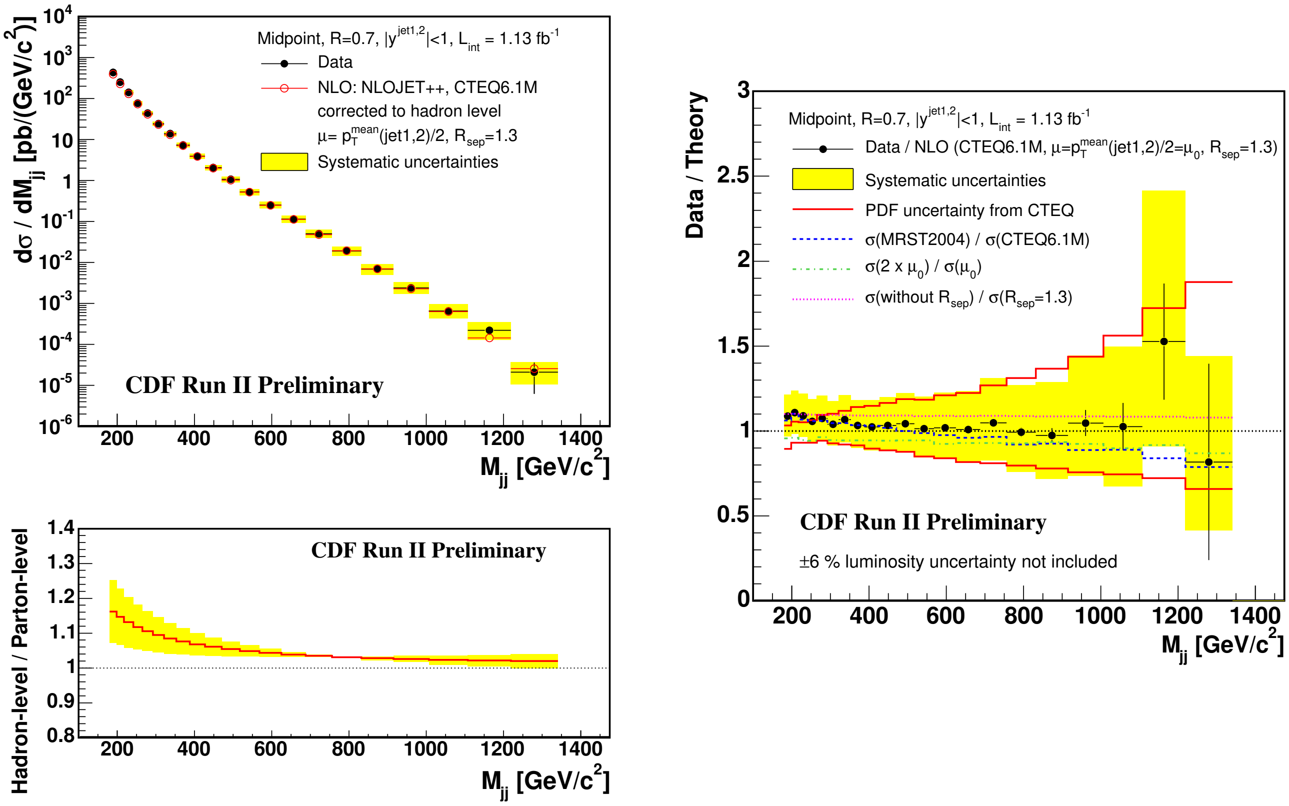

FIG. 1: (top left) The measured dijet mass spectra for jets with $|y^{jet1,2}| < 1$ compared to the NLO pQCD predictions based on CTEQ6.1 PDF. (bottom left) The non-perturbative parton-to-hadron level bin-by-bin corrections. (left) The ratio of the data to the NLO pQCD predictions corrected by the parton-to-hadron level correction. The experimental uncertainties, theoretical uncertainties from PDF, the ratio of MRST2004/CTEQ6.1, and the dependence on the choice of μ scale and R_{sep} are also shown.

determined to be 96% from the beam profile measured using a minimum bias sample.

The jet energies measured by the calorimeters are affected by instrumental effects, such as calorimeter non-uniformity, non-linearity and energy smearing. We correct for these biases in several steps [15]. First, an η-dependent relative correction is applied to equalize in η the response of the CDF calorimeters to jets. The equalized jet p_T is then corrected for the pileup effect, *i.e.*, the effect of additional $p\bar{p}$ interactions in the same bunch crossing. Then, the average p_T-dependent correction is applied to correct on average the undermeasured hadron energy due to the non-linearity of the CDF calorimeters. After these corrections, we sort jets in decreasing p_T and reconstruct dijet mass, m_{jj}, using the two highest p_T jets, and then we can form the dijet mass spectrum as:

$$\frac{d\sigma}{dm_{jj}} = \frac{1/\epsilon_{trig,i}}{\mathcal{L}_i} \frac{N_{event,i}}{\Delta m_{jj,i}} \tag{1}$$

where $N_{event,i}$ is the number of events, in the i-th dijet mass bin, $\epsilon_{trig,i}$ is the trigger efficiency and $\Delta m_{jj,i}$ is the width of the i-th dijet mass bin. $\mathcal{L}_i$ is the integrated luminosity of the trigger sample used for the i-th dijet mass bin.

In order to compare the measured dijet mass spectrum with the QCD prediction for dijet production at the hadron level, the measured spectrum must be further corrected for the bin-by-bin migration effect due to finite resolution in the m_{jj} measurement and the efficiencies of the offline event selection requirements. The unfolding correction is determined on a bin-to-bin basis using PYTHIA events that have passed through the CDF detector simulation by taking a ratio of the binned hadron level cross section and calorimeter level cross section. The corrected dijet mass spectrum is shown in Fig 1 together with the statistical and systematic uncertainties. The systematic uncertainties arise mainly from three sources: the jet energy scale, the jet energy resolution, and the luminosity.

The measured spectrum is compared to the next-to-leading order perturbative QCD (NLO pQCD) predictions from fastNLO which is based on the NLOJET++ program. For the parton distribution function (PDF) in the proton, CTEQ6.1 is used, and the renormalization and factorization scales are set to the average p_T of the leading two jets. In

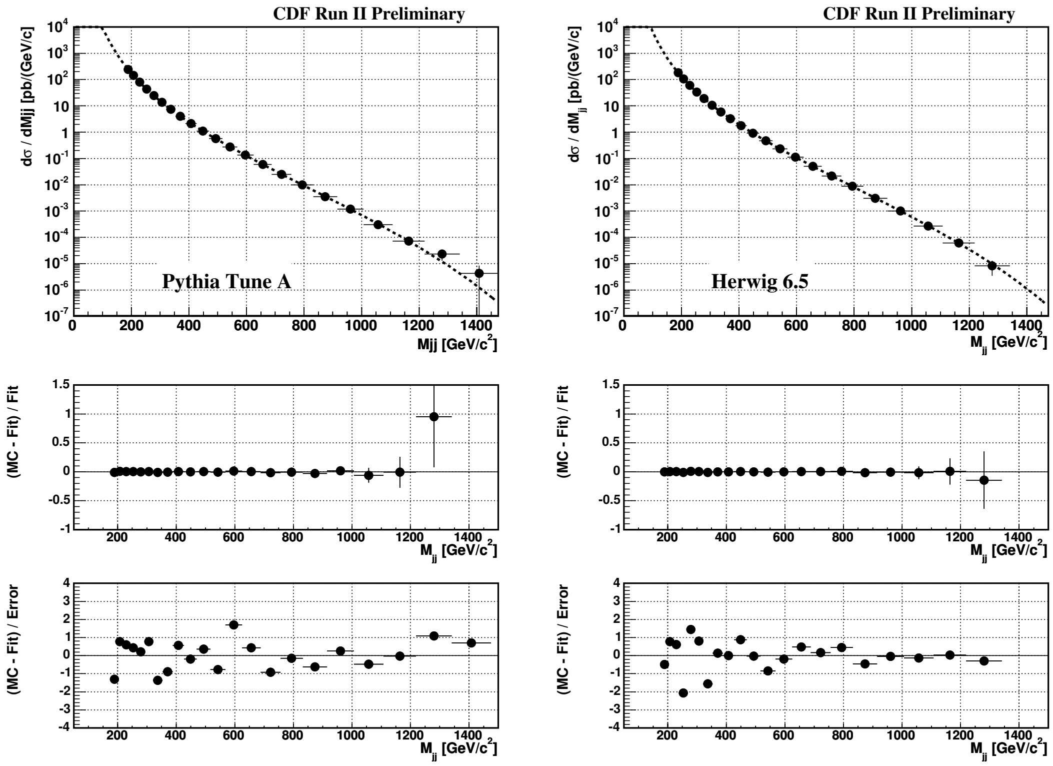

FIG. 2: (top) The dijet mass spectra for jets with $|Y1, 2| < 1$ from the PYTHIA Tune A (left) and HERWIG (right) dijet Monte Carlo samples. The (data-fit)/fit and (data-fit)/error versus dijet mass are shown in the middle and bottom plots, respectively.

order to mimic the the properties of the splitting/merging step which is present in the experimental measurement but not in NLO pQCD calculation, a parameter of $R_{sep} = 1.3$ is introduced. Two partons are clustered into a single jet, if they are within $R_{cone} = 0.7$ of the jet centroid and within $R_{sep} \times R_{cone}$ of each other. The NLO pQCD predictions for jets of partons are corrected for the non-perturbative underlying and hadronization effects which derived by running the jet clustering algorithm to the hadron level and parton level outputs of the PYTHIA Monte Carlo samples, generated with and without an underlying event. The bin-by-bin non-perturbative correction and the ratio of the measured spectrum to the NLO pQCD predictions corrected for the non-perturbative effects are shown in Fig 1. Also shown are the uncertainties due to PDF based on 40 CTEQ6.1 PDFs, and the data and theoretical predictions are found to be in good agreement.

IV. SEARCH FOR DIJET MASS RESONANCES

We search for narrow mass resonances in the measured dijet mass spectrum by fitting the measured spectrum to a smooth parametrization form and by looking for data points which show significant excess from the fit. We use the following parametrization form:

$$\frac{d\sigma}{dm} = p_0(1-x)^{p_1}/x^{p_2+p_3\cdot\ln(x)}, \quad x = m_{jj}/\sqrt{s}. \tag{2}$$

which was found to fit well the dijet mass spectra from PYTHIA and HERWIG MC events as well as from NLO pQCD. The fit of the parametrization form (2) to the PYTHIA Tune A [16] and HERWIG samples are shown in Fig. 2. We fit the measured dijet mass spectrum before the bin-by-bin corrections for the migration effects are made, in order to get rid of the bin-to-bin fluctuation in the correction. The dijet mass spectrum measured in data are fitted to the parametrization (2), and the results are shown in Fig. 3. We find no evidence for existence of new massive particles. Therefore, we proceed to set limits on new particle production below.

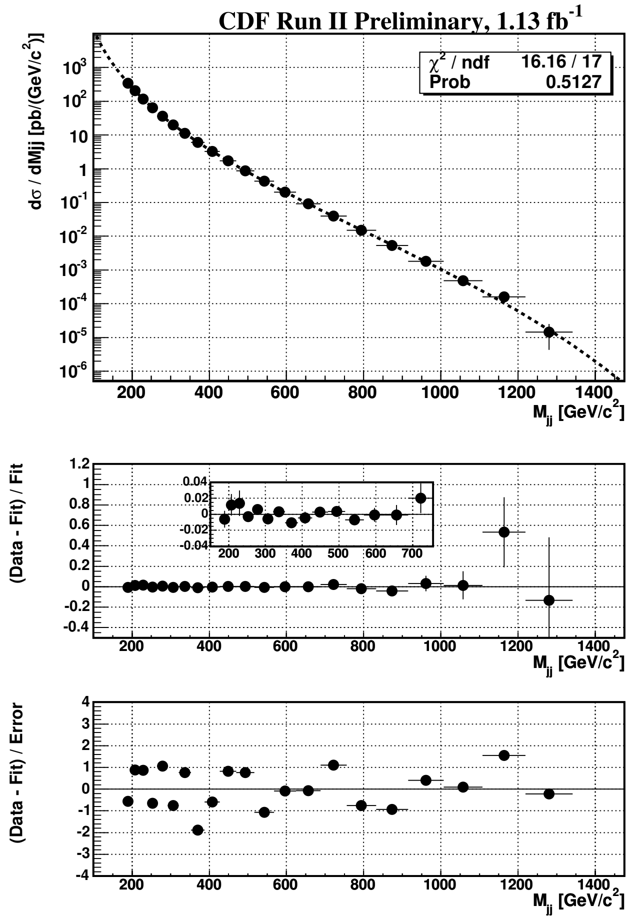

FIG. 3: (top) The measured dijet mass spectrum fitted to the Eq. (2). (middle) (data-fit)/fit as a function of m_{jj}. The inset shows the blow-up view in which the vertical scale is restricted to ± 0.04. (bottom) (data-fit)/(statistical error on data) as a function of m_{jj}.

V. LIMITS ON NEW PARTICLES

The following models have been considered in this dijet mass resonance search. The quark compositeness model predicts the existence of the excited quarks that decay into a quark and a gluon ($q^* \to qg$) [1]. We consider the standard model couplings $f = f' = f_s = 1$ and set the compositeness scale to the mass of the excited quark. We also consider $W'(\to q\bar{q}')$ and $Z'(\to q\bar{q})$ with the standard model couplings. Another model considered is the Randall-Sundrum graviton production ($G \to q\bar{q}, gg$) [5] with the parameter $k/\bar{M}_{pl} = 0.1$. The leading-order production cross section of W', Z' and Randall-Sundrum gravitons are multiplied by a factor of 1.3 to account for higher-order effects in α_s. The models were simulated with PYTHIA with the Tune A parameters and the CDF detector simulation. Figure 4 shows the dijet mass spectrum prediction from NLO pQCD and the dijet mass line shapes from the excited quarks, W', Z' and Randall-Sundrum gravitons for $M = 300, 500, 700, 900$ and 1100 GeV. The dijet mass line shapes from the mass of 800 GeV/c^2 are also compared to each other in Fig. 5. The dijet mass line shapes are broader for the the excited quarks and Randall-Sundrum gravitons than for W' and Z' because the excited quarks and Randall-Sundrum gravitons can decay into the mode containing gluons unlike W' and Z'; gluons radiate more than quarks and tend to make the resulting dijet mass line shapes broader. Therefore, the cross section limits obtained based on the excited quark and Randall-Sundrum graviton line shapes are about 20% larger than those obtained with the W' and Z' line shapes.

We also considered the axigluons and flavor-universal colorons ($A \to q\bar{q}$) [2], E_6 diquark ($D(D^c) \to (qq)\bar{q}\bar{q}$) [4], and the color-octet techni-ρ [3] production; their lowest-order theoretical predictions for the cross section times the branching ratio are evaluated at the parton level and shown in Fig. 6 along with the predictions for the other models described above as a function of new particle mass. For the color-octet techni-ρ production, the predictions are for

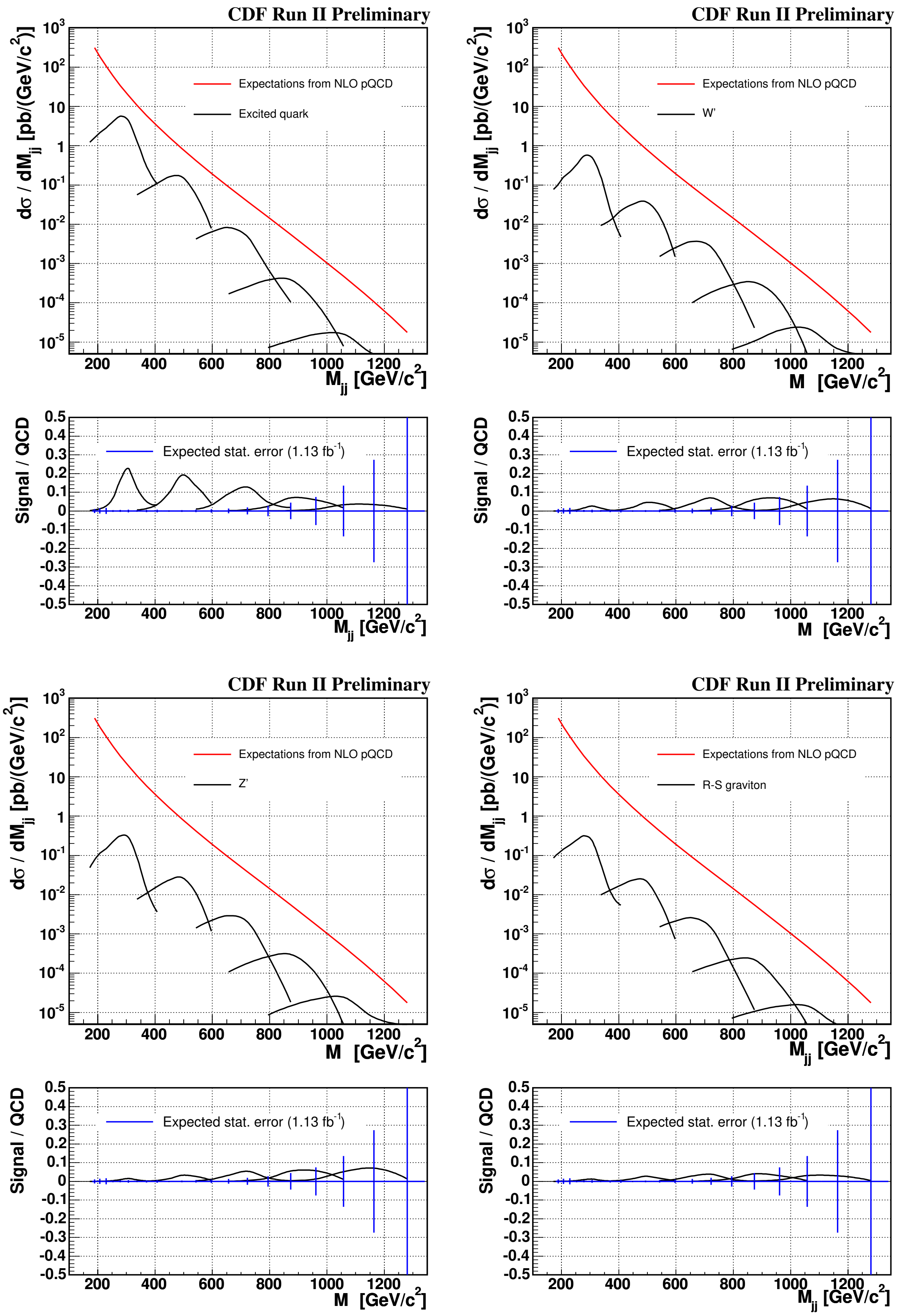

FIG. 4: The QCD dijet mass spectrum from NLO pQCD and the dijet mass line shapes in the (top left) excited quark, (top right) W', (bottom left) Z' and (bottom right) Randall-Sundrum gravitons for $M = 300, 500, 700, 900$ and 1100 GeV$/c^2$.

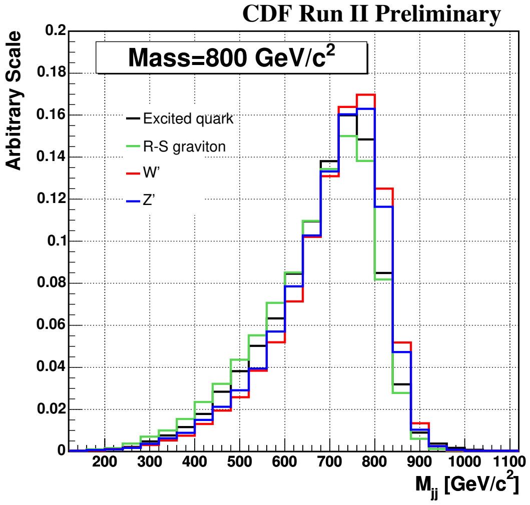

FIG. 5: Dijet mass distributions in q^*, W', Z' and Randall-Sundrum graviton Monte Carlo events for the input mass of 800 GeV/c^2.

the mass degenerate techni-ρ with the standard topcolor-assisted-technicolor (TC2) couplings and with the following parameter settings: $M_8' = 0$, $M(\pi_{22}^8) = 5M(\rho)/6$, $M(\pi_{22}^1) = M(\pi_{22}^8)/2$ and $M_8 = 5M(\rho)/6$. The new particle decay angular distributions are included in the predictions, and we require $|y^{jet1,2}| < 1$ for all predictions.

We set an upper limit on the cross section using the likelihood function:

$$L = \prod_i \frac{\mu_i^{n_i} \exp(-\mu_i)}{n_i!}, \tag{3}$$

where

$$\mu_i = \sigma(\text{signal})\mathcal{L}\epsilon_i n_i^{sig}/n_{tot}^{sig} + N_i(\text{QCD}). \tag{4}$$

n_i is the observed number of events in the i-th dijet mass bin, μ_i is the "predicted" number of events in the i-th dijet mass bin, $\mathcal{L}$ is the integrated luminosity, ϵ_i is the event selection cut efficiencies in the i-th dijet mass bin, and n_i^{sig}/n_{tot}^{sig} is for the signal line shape, *i.e.* the ratio the numbers of signal events in the i-th dijet mass bin to the total number of signal events. The event selection cut efficiencies, ϵ_i, include the z_{vtx} cut efficiencies, missing E_T significance cut efficiencies as well as the trigger efficiencies. We consider that the QCD background is a smooth function given by the parametrization in Eq. (2), and this provides the predicted number of background events in the i-th dijet mass bin, N_i(QCD).

We set upper limits on the new particle production cross section times the branching ratio times the kinematic acceptance that the produced leading two jets are within $|y^{jet1,2}| < 1$ [*i.e.*, $\sigma \times Br \times Acc(|y^{jet1,2}| < 1)$], by forming the likelihood distribution as a function of $\sigma \times Br \times Acc(|y^{jet1,2}| < 1)$ at each new particle mass. We maximize the likelihood with respect to the four parameters in the QCD background parametrization Eq. (2) by keeping these parameters free, since they are not *a priori* constrained. The systematic uncertainties due to jet energy scale, jet energy resolution, luminosity, trigger efficiencies, and prescale factors are taken into account when the limits are computed using the Bayesian approach by convoluting the likelihood function with a truncated Gaussian prior distribution for each uncertainty.

The obtained limits using the W', Z', the excited quark, and the Randall-Sundrum graviton line shapes are shown in Fig. 6 as a function of the new particle mass. Also shown are the theoretical predictions for the various models for the production of new particle that decay into dijets. For W', Z', excited quarks and Randall-Sundrum gravitons, the mass exclusion is determined by comparing the limits obtained with their respective signal shapes and cross section predictions. For the axigluons, flavor-universal colorons, and E_6 diquarks, we compare their cross section predictions with the limits obtained with the excited quark signal shapes; these particles do not decay into the mode containing a gluon, so their signal shape would be narrower than the excited quark, and thus the limits obtained with the excited quark signal shapes are somewhat conservative. For the color-octet techni-ρ, we compare the cross section predictions with the limits obtained with the Randall-Sundrum graviton signal shapes. The color-octet techni-ρ and Randall-Sundrum graviton decay channels are similar; the branching fraction to the gg state is higher for the Randall-Sundrum

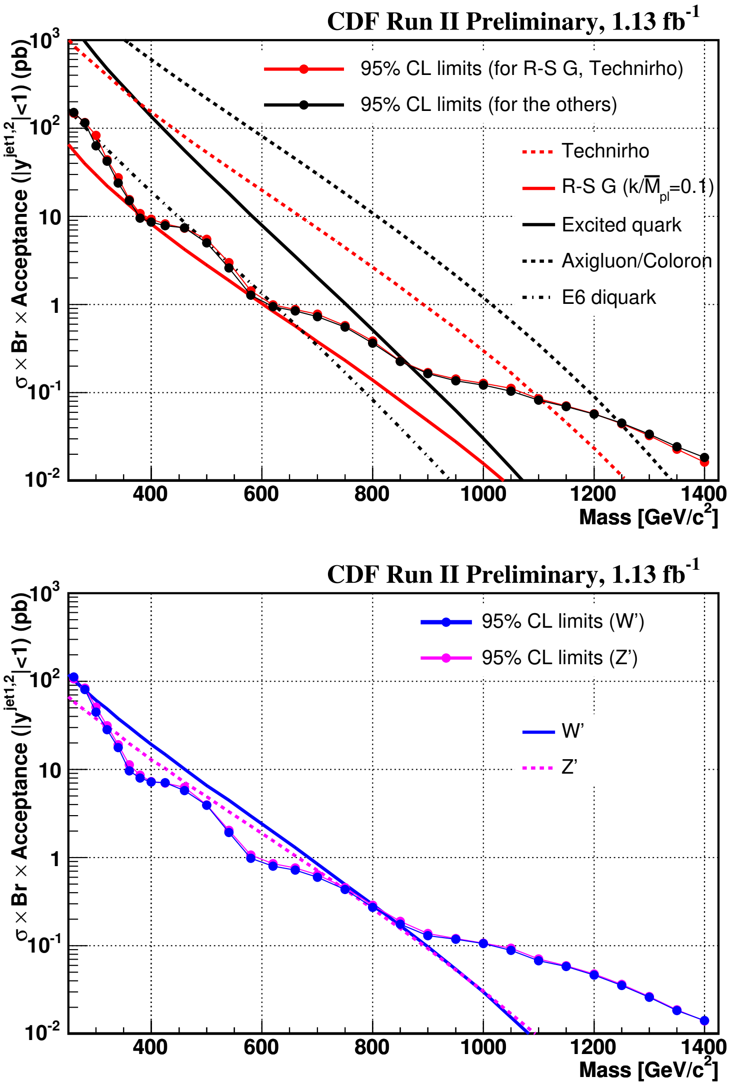

FIG. 6: Observed 95% C.L Upper limits on the new particle production cross sections obtained with the signal shapes from the color-octet techni-ρ, W', Z' and excited quark production compared with the cross section predictions for the excited quark ($f = f' = f_s = 1$), Axigluon, coloron ($\cot\theta = 1$), color octet techni-ρ (for the set of parameters described in the text), E_6 diquark, sequential W', Z', and Randall-Sundrum graviton ($k/\bar{M}_{pl} = 0.1$).

gravitons than for the color-octet techni-ρ, so the limits obtained with the Randall-Sundrum graviton signal shapes are conservative. The mass exclusion regions for all the new particles considered are:

- $260 < m < 870$ GeV/c^2 for the excited quark ($f = f' = f_s = 1$),
- $260 < m < 1250$ GeV/c^2 for the axigluon and flavor-universal coloron (mixing of two $SU(3)$, $\cot\theta = 1$), and
- $290 < m < 630$ GeV/c^2 for the E_6 diquark,
- $260 < m < 1100$ GeV/c^2 for the color-octet techni-ρ [mass degenerate techni-ρ with standard topcolor-assisted-technicolor (TC2) couplings, $M_8' = 0$, $M(\pi_{22}^8) = 5M(\rho)/6$, $M(\pi_{22}^1) = M(\pi_{22}^8)/2$, $M_8 = 5M(\rho)/6$],
- $280 < m < 840$ GeV/c^2 for sequential W',
- $320 < m < 740$ GeV/c^2 for sequential Z',

respectively. For the Randall-Sundrum gravitons, we could not exclude any mass region. This searches set the most stringent upper limits on the production of the excited quark, axigluon, the flavor-universal coloron, E_6 diquark, and color-octet techni-ρ to date.

Acknowledgments

We thank the Fermilab staff and the technical staffs of the participating institutions for their vital contributions. This work was supported by the U.S. Department of Energy and National Science Foundation; the Italian Istituto Nazionale di Fisica Nucleare; the Ministry of Education, Culture, Sports, Science and Technology of Japan; the Natural Sciences and Engineering Research Council of Canada; the National Science Council of the Republic of China; the Swiss National Science Foundation; the A.P. Sloan Foundation; the Bundesministerium fuer Bildung und Forschung, Germany; the Korean Science and Engineering Foundation and the Korean Research Foundation; the Particle Physics and Astronomy Research Council and the Royal Society, UK; the Russian Foundation for Basic Research; the Comision Interministerial de Ciencia y Tecnologia, Spain; and in part by the European Community's Human Potential Programme under contract HPRN-CT-20002, Probe for New Physics.

---

[1] U. Baur, I. Hinchliffe and D. Zeppenfeld, Int. J. Mod. Phys. A **2**, 1285 (1987).
U. Baur, M. Spira and P. M. Zerwas, Phys. Rev. D **42**, 815 (1990).
[2] J. Bagger, C. Schmidt and S. King, Phys. Rev. D **37**, 1188 (1988).
P. H. Frampton and S. L. Glashow, Phys. Lett. B **190**, 157 (1987).
[3] K. D. Lane and M. V. Ramana, Phys. Rev. D **44**, 2678 (1991).
E. Eichten and K. D. Lane, Phys. Lett. B **327**, 129 (1994).
K. Lane and S. Mrenna, Phys. Rev. D **67**, 115011 (2003).
[4] J. L. Hewett and T. G. Rizzo, Phys. Rept. **183**, 193 (1989).
[5] L. Randall and R. Sundrum, Phys. Rev. Lett. **83**, 3370 (1999).
J. Bijnens, P. Eerola, M. Maul, A. Mansson and T. Sjostrand, Phys. Lett. B **503**, 341 (2001).
[6] J. Alitti *et al.* (UA2 Collaboration), Z. Phys. C **49**, 17 (1991).
[7] J. Alitti *et al.* (UA2 Collaboration), Nucl. Phys. B **400**, 3 (1993).
[8] F. Abe *et al.* (CDF Collaboration), Phys. Rev. Lett. **74**, 3538 (1995).
[9] F. Abe *et al.* (CDF Collaboration), Phys. Rev. D **55**, 5263 (1997).
[10] V. M. Abazov *et al.* (DØ Collaboration), Phys. Rev. D **69**, 111101 (2004).
[11] A. Abulencia *et al.* (CDF Collaboration), J. Phys. G **34**, 2457 (2007).
[12] G. C. Blazey *et al.* (2000), hep-ex/0005012.
[13] A. Abulencia *et al.* (CDF Collaboration), Phys. Rev. D **74**, 071103 (2006).
[14] The missing transverse energy ($\vec{\not\!\!E}_T$) is defined by, $\vec{\not\!\!E}_T = -\sum_i E_T^i \hat{\mathbf{n}}_\mathbf{i}$, where $\hat{\mathbf{n}}_\mathbf{i}$ is a unit vector perpendicular to the beam axis and pointing at the ith calorimeter tower. The sum is over all the calorimeter towers with $E_T > 100$ MeV and $|\eta| < 3.6$. We define the missing E_T significance as $|\vec{\not\!\!E}_T|/\sqrt{\sum_i E_T^i}$.
[15] A. Bhatti *et al.*, Nucl. Instrum. Methods Phys. Res. A **566**, 375 (2006).
[16] R. Field, presented at *Fermilab ME/MC Tuning Workshop*, Fermilab, October 4, 2002. PYTHIA Tune A implies that the following parameters are set in PYTHIA with CTEQ5L: PARP(67)=4, MSTP(82)=4, PARP(82)=2, PARP(84)=0.4, PARP(85)=0.9, PARP(86)=0.95, PARP(89)=1800, PARP(90)=0.25. These parameters were tuned to reproduce the energy observed in the region transverto the leading jet in the jet data from Run I.
[17] T. Aaltonen *et al.* (CDF Collaboration), Phys. Rev. Lett. **99**, 171801 (2007).
[18] T. Aaltonen *et al.* (CDF Collaboration), Phys. Rev. Lett. **99**, 171802 (2007).